Tachikawa, T., Minohara, M., Bell, C., & Hwang, HY. (2015). Tuning band alignment using interface dipoles at the Pt/anatase TiO_2 interface. *Advanced Materials*, *27*(45), 7458-7461. https://doi.org/10.1002/adma.201503339

Tuning band alignment using interface dipoles at the Pt/anatase TiO_2 interface

Takashi Tachikawa, Makoto Minohara, Yasuyuki Hikita, Christopher Bell, Harold Y. Hwang*

Dr. T. Tachikawa, Dr. Y. Hikita, Prof. H. Y. Hwang
Stanford Institute for Materials and Energy Sciences, SLAC National Accelerator Laboratory
2575 Sand Hill Road, Menlo Park, California, 94025, USA.
E-mail: hikita@stanford.edu

Dr. T. Tachikawa
Department of Advanced Materials Science, The University of Tokyo
5-1-5 Kashiwanoha, Kashiwa, Chiba, 277-8561, Japan.

Dr. M. Minohara
Photon Factory, Institute of Materials Structure Science, High Energy Accelerator Research Organization
1-1 Oho, Tsukuba, Ibaraki, 305-0801, Japan.

Dr. C. Bell
School of Physics, University of Bristol
H. H. Wills Physics Laboratory, Tyndall Avenue, Bristol, BS8 1TL, UK.

Prof. H. Y. Hwang
Department of Applied Physics, Geballe Laboratory for Advanced Materials, Stanford University
476 Lomita Mall, Stanford University, Stanford, California, 94305, USA.

Keywords: (transition metal oxides, TiO_2, band alignment, interface dipoles, $LaAlO_3$)

Atomic scale control of epitaxial transition metal oxide heterostructures have led to novel strategies to design interface devices, as well as providing a platform for exploring emergent electronic ground states.[1] Due to the strong ionic bonding in oxides, one of the central features in oxide heterostructures is the design and manipulation of their polar surfaces especially as they are brought into contact with a non-polar surface forming a so-called "polar interface".[2] At polar interfaces, several electrostatically induced effects are known to occur. One example is the stabilization of large electrostatic potential as recently reported in (001)-oriented perovskite Schottky junctions between metallic $SrRuO_3$ and semiconducting $SrTiO_3$.[3] By inserting ultrathin $LaAlO_3$ layers at this non-polar interface, epitaxially

stabilized alternate stacking of $(LaO)^+$ and $(AlO_2)^-$ charged layers naturally form a dipole effectively modifying the Schottky barrier height (SBH) by as much as 1 eV. Another manifestation of electrostatics at oxide polar interfaces is the electronic reconstruction driven to minimize the high electrostatic energy as seen in the generation of confined high mobility electron channels at the $LaAlO_3/SrTiO_3$ (100) interface,[4] and variation in the electronic states in $LaAlO_3/LaVO_3/LaAlO_3$ (001) quantum wells.[5] Up to now, the study of polar interfaces and the associated electrostatic boundary conditions have primarily been limited to isostructural perovskite interfaces. In this regard, the recent observation of substrate termination dependent conductivity in the anatase $TiO_2/LaAlO_3$ (001) heterostructure suggests the importance of electrostatics even at non-isostructural binary oxide interfaces.[6] These studies motivate us to examine the feasibility of dipole engineering of SBHs in binary oxide heterostructures given their significant role in a wide variety of device applications.

In this study, we focus on the interface between polycrystalline Pt metal and single crystalline anatase TiO_2 thin film as a model system, and examine the impact of inserting a perovskite dipole layer, $LaAlO_3$, to control the Pt/TiO_2 (001) SBH as shown in **Figure 1**. All of our heterostructures were fabricated on $LaAlO_3$ (001) substrates. Anatase TiO_2 is a promising material for various applications such as transparent electrodes, photocatalysts, resistive memories, and solar cells.[7-9] In all of these, insertion of dipole layers to control band alignments can dramatically affect the device performance. By inserting < 1 nm of a perovskite $LaAlO_3$ in the [001] orientation, we successfully achieved a modulation in the SBH from 1.6 eV to 0.8 eV at this Pt/anatase TiO_2 (001) interface.

This work is based on overcoming several important technical challenges. Firstly it is known that the anatase TiO_2 phase can be unstable when $LaAlO_3$ is overgrown in various growth conditions.[10,11] In order to stabilize high quality $LaAlO_3/TiO_2$ (001) heterostructures, we investigated the mechanism of TiO_2 crystalline quality degradation after subsequent $LaAlO_3$ overgrowth. For a partial oxygen pressure $P_{O2} = 1 \times 10^{-5}$ Torr, the anatase TiO_2

grown on $LaAlO_3$ (001) is stable up to 750 ^oC, above which the rutile phase begins to form due to its higher thermodynamic stability.[12] We set the temperature and the oxygen pressure during $LaAlO_3$ growth to similar conditions used for the TiO_2 growth to prevent the anatase to rutile transition. However, these thermodynamic conditions differ from those typically used for high quality $LaAlO_3$ films,[13] therefore we varied the growth *kinetics* by optimizing the growth rate, which have been shown to be effective in the pulsed laser deposition of oxides previously.[14,15]

Structural and electrical characterization of $LaAlO_3$ (40 unit cell, u.c.)/TiO_2 (40 u.c.)/$LaAlO_3$ (001) heterostructures with various laser repetition rates of $LaAlO_3$ are summarized in **Figure 2 A-C**. Relatively thick $LaAlO_3$ was used for the optimization to precisely characterize the quality of this layer. The x-ray diffraction (XRD) peak intensity of anatase TiO_2 (004) monotonically decreased with increasing laser repetition rate during $LaAlO_3$ growth (Figure 2 A). The Raman scattering spectra in Figure 2 B show that the $LaAlO_3$ grown at relatively high growth rate reduces the anatase A_{1g} and E_g mode intensities, consistent with the decrease in anatase XRD peak intensity. At the fastest growth rate, relatively weak signatures of rutile A_{1g}, B_{1g}, and E_g modes begin to appear on a large background signal in the Raman scattering spectrum suggesting the conversion of TiO_2 towards the thermodynamically stable phase.

In order to understand the origin of the structural degradation of TiO_2, electrical transport measurements were performed as shown in Figure 2 C. From Hall measurements at room temperature, the average electron density monotonically increases with the laser repetition rate used for $LaAlO_3$ growth. Since there is negligible electrical conduction in $LaAlO_3$ at room temperature, these results suggest that the $LaAlO_3$ grown at relatively high growth rate induces more oxygen vacancies and hence electrons in TiO_2.[16] This can be explained by a competition between oxygen incorporation from the atmosphere and oxygen extraction from the underlying TiO_2 layer.[17] For high-growth rates, the ablated $LaAlO_3$

species have insufficient time to fully oxidize with the oxygen atmosphere on the TiO_2 surface and oxygen deficiency in $LaAlO_3$ is compensated by oxygen gettering from the TiO_2 layer. This is consistent with the higher electronegativity of Ti^{4+} in TiO_2 than Al^{3+} in $LaAlO_3$.[18] At a lower growth rate, in this case a laser repetition rate of 0.6 Hz, the carrier density measured in the $LaAlO_3/TiO_2$ heterostructure is the same as that of a TiO_2 film without $LaAlO_3$ capping, indicating no measurable degradation in the crystalline quality in the TiO_2 underlayer consistent with the XRD results.

The second challenge is matching the in-plane lattice symmetry at the $LaAlO_3/TiO_2$ (001) thin film interface. The surface of anatase TiO_2 (001) thin film after growth in UHV typically shows a (1 × 4) reconstructed reflection high-energy electron diffraction (RHEED) pattern as shown in the left image in **Figure 2 D**. Experimentally, we found that dosing this surface *ex situ* with deionized water at room temperature and drying in air for 2 hours converted the RHEED pattern to a (1 × 1) surface which was preserved even up to 625 ^{o}C in P_{O2} = 1 ×10^{-5} Torr, above the growth temperature for the $LaAlO_3$ overlayers (right image in Figure 2 D). We note that the intrinsic (1 × 4) surface is substantially more stable than that of a pristine (1 × 1) surface.[19] We suggest that the observed transition in the RHEED pattern is caused by dissociative water adsorption on the (1 × 4) surface as predicted by theory,[19] or due to the airborne carbon contamination.[20]

The Schottky junctions for barrier height characterization were prepared by evaporating polycrystalline Pt metal on top of the $LaAlO_3/TiO_2$ (001) heterostructures employing slow growth rate for $LaAlO_3$ deposition on water treated TiO_2 (001) thin films. The $LaAlO_3$ thickness was varied between 0 u.c. and 2 u.c. and a Nb = 0.3 at. % doped TiO_2 (Nb:TiO_2) target was used instead of non-doped TiO_2 to introduce carriers uniformly across the thin film. The water treatment was successfully applied to the Nb-doped films to produce the (1 × 1) RHEED pattern as observed for the non-doped case.

From current-voltage measurements at room temperature, clear rectification was confirmed indicating that all junctions have a Schottky barrier between Pt and TiO_2 (not shown). Capacitance voltage (*C-V*) measurements were performed to obtain the built-in potential (V_{bi}) as shown in **Figure 3 A**. For all cases, C^{-2} is linearly proportional to the applied bias, which is typical behavior of Schottky junctions. V_{bi}, obtained by the voltage intercept of the linear extrapolation of $C^{-2} - V$, decreases linearly with the thickness of $LaAlO_3$ suggesting an active role of $LaAlO_3$ as a dipole layer. It should be noted that there is no V_{bi} shift in the case of 1 u.c. $LaAlO_3$ deposited on a (1 × 4) Nb:TiO_2 (001) surface, indicating that the (1 × 1) Nb:TiO_2 (001) surface is crucial in obtaining the dipole offset. From the $C^{-2} - V$ slope, we obtain a mean dopant concentration in the Nb:TiO_2 film of 1.5×10^{19} cm^{-3} with 20 % variation with varying the dipole layer thickness, which is characteristic of the sample-to-sample variation.

Internal photoemission (IPE) was also utilized to directly measure the SBH. The square root of the photoyield (*Y*), defined as the photocurrent generated per photon, is shown in **Figure 3 B** as a function of the incident photon energy. The square root of the photoyield was linearly fitted and extrapolated to the photon energy intercept to obtain the SBH. The SBHs monotonically decreased with increasing $LaAlO_3$ thickness. The values obtained from IPE and *C-V* are summarized in **Figure 4** showing good agreement with each other. To understand these data, we note that $LaAlO_3$ is a robust insulator in bulk, and hence Pt/$LaAlO_3$/Nb:TiO_2 (001) can be regarded as a metal insulator semiconductor (MIS) junction. In this case, the built-in potential in the Nb:TiO_2 is expressed as

$$V_{bi} = V_0 - \frac{\varepsilon_{TiO2} q N_d}{C_{LaAlO3}^{\ 2}} \left(\sqrt{1 + \frac{2 V_0 C_{LaAlO3}^{\ 2}}{\varepsilon_{TiO2} q N_d}} - 1 \right), \quad (1)$$

where ε_{TiO2} and N_d are the dielectric constant and the dopant concentration in Nb:TiO_2 respectively, C_{LaAlO3} is the capacitance of the $LaAlO_3$, and V_0 is the built-in potential of a

Pt/Nb:TiO_2 junction without $LaAlO_3$. As the $LaAlO_3$ thickness increases, C_{LaAlO3} decreases thus decreasing the built-in potential in the Nb:TiO_2. However, based on the $LaAlO_3$ and the anatase TiO_2 dielectric constants of 28 and 30, C_{LaAlO3} for 0.4 nm-thick $LaAlO_3$ is 50 times larger than that of the ~20 nm-thick Nb:TiO_2 depletion layer capacitance.[21,22] Therefore, the measured V_{bi} drop induced by the capacitance of $LaAlO_3$ is less than 0.1 V and cannot explain the large V_{bi} change obtained from the *C-V* data. Instead we can understand these results if we assume that a dipole is formed by the $LaAlO_3$ layer growing on the Nb:TiO_2, whose sign is consistent with the first atomic layer being $(LaO)^+$. This is in agreement with first principles calculations which indicate higher stability for the LaO/TiO_2 interface over the AlO_2/TiO_2 interface.[23]

As an independent test of our hypothesis that the SBH change is attributed to the interface dipoles, two other perovskites having different average sheet charge densities were inserted at the Pt/Nb:TiO_2 (001) interface. We utilized $SrZrO_3$ and $(LaAlO_3)_{0.5}(SrTiO_3)_{0.5}$ for the insertion layers which, in a simple ionic picture, can be regarded as an alternate stacking of $(SrO)^0/(ZrO_2)^0$ and $(La_{0.5}Sr_{0.5}O)^{0.5+}/(Al_{0.5}Ti_{0.5}O_2)^{0.5-}$ in the [001] direction respectively. Since the dielectric constant of $SrZrO_3$ and $(LaAlO_3)_{0.5}(SrTiO_3)_{0.5}$ are approximately the same as $LaAlO_3$, their dipole moments are expected to be 0 and 0.5 times that of $LaAlO_3$, respectively.[24,25] The SBH reductions induced by these dipole layers are summarized in Figure 4. The gradient of the SBH reduction vs. $(LaAlO_3)_{0.5}(SrTiO_3)_{0.5}$ thickness is half of that of $LaAlO_3$ and in the case of $SrZrO_3$, the SBH showed almost no change with the layer thickness. These trends are strongly indicative of dipole tuning of the SBH by the ionic charges in the interlayer. We note that oxygen extraction from Nb:TiO_2 into the dipole layer can also be an alternative origin for the reduction in SBH. However, under the growth conditions employed in our study, the generated oxygen vacancies are far insufficient to reproduce the observed large modulation range in SBH. Furthermore, the similar electronegativity of Zr^{4+} and Al^{3+} would predict comparable amount of oxygen vacancy

generation in Nb:TiO_2, which cannot account for the contrasting modulation in SBH between $SrZrO_3$ and $LaAlO_3$.

In summary, we successfully engineered the Pt/Nb:TiO_2 (001) Schottky barrier heights by insertion of ultrathin perovskite dipole layers enabling the modulation of SBH proportional to the dipole magnitude of the polar layers. The capability to tailor barrier heights independent of the constituent materials should be a powerful tool in designing functional devices in binary oxide systems.

Experimental Section

$LaAlO_3$/TiO_2 (001) heterostructures were epitaxially grown on $LaAlO_3$ (001) substrates by using pulsed laser deposition (PLD) with a KrF excimer laser (pulse duration ~ 20 ns) imaged onto a rectangular spot size of 0.04 cm^2. Prior to deposition, the substrates were annealed at 900 ºC and P_{O2} = 1 × 10^{-6} Torr to obtain atomically flat surfaces. The 40 nm thick TiO_2 and Nb:TiO_2 (Nb = 0.3 at. %) thin films were deposited by ablating a polycrystalline target at the substrate temperature and oxygen pressure of 700 ºC and P_{O2} = 1 × 10^{-5} Torr, respectively. The laser energy density and repetition rate was 0.6 J/cm^2 and 1 Hz, which were optimized to suppress oxygen vacancies in the TiO_2 thin films.[15] $LaAlO_3$ thin films were grown on TiO_2 at 600 ºC and P_{O2} = 1 × 10^{-5} Torr. The laser fluence was fixed to 0.36 J/cm^2 and the repetition rate was varied from 0.6 Hz to 3 Hz. During the entire growth of the $LaAlO_3$/TiO_2 heterostructures, RHEED was used to confirm the surface crystallographic structure and the growth thickness from the intensity oscillations.[26] The evaluated thickness showed good correspondence with the X-ray reflectivity measurement taken after growth. The $SrZrO_3$ and $(LaAlO_3)_{0.5}(SrTiO_3)_{0.5}$ dipole layers were fabricated at 600 ºC and P_{O2} = 1 × 10^{-5} Torr using the laser fluence of 0.44 J/cm^2 and a repetition rate of 1 Hz. The surface topographies of oxide films were confirmed by atomic force microscopy and the obtained root mean square was

approximately 2 nm. Micro Raman scattering spectroscopy equipped with a 532 nm green laser for excitation was utilized to determine the dominant phase present in the TiO_2 films.

Schottky contacts were fabricated by evaporating 5 nm of Pt metal using an electron beam evaporator at room temperature and in high vacuum (3×10^{-7} Torr) through a shadow mask. The growth rate of Pt was fixed at 0.01 nm/s and monitored *in situ*. Ohmic contacts were made using bonded Al-wires on the dipole engineered Nb:TiO_2 surface. Impedance measurements and DC current-voltage measurements were performed in air at room temperature. The capacitance was extracted from the measured impedance by assuming one capacitor in parallel with one resistor for all measurements. The fitting was carried out in the range of voltage where the dissipation was less than 0.4. For IPE, a tungsten-halogen light source equipped with a grating monochromator was used as the light source and the photocurrent detection was carried out using a lock-in amplifier synchronized with an optical chopper.

Acknowledgements

This work is supported by the Department of Energy, Office of Basic Energy Sciences, Division of Materials Sciences (Y.H. and H.Y.H) and Engineering, and Laboratory Directed Research and Development funding (Y.H.), under contract DE-AC02-76SF00515.

Received: ((will be filled in by the editorial staff))
Revised: ((will be filled in by the editorial staff))
Published online: ((will be filled in by the editorial staff))

[1] J. Mannhart and D. G. Schlom, Science **2010**, 327, 1607.

[2] C. Noguera, J. Phys. Condens. Matter **2000**, 12, R367.

[3] T. Yajima, M. Minohara, C. Bell, H. Kumigashira, M. Oshima, H. Y. Hwang, Y. Hikita, Nano Lett. **2015**, 15, 1622.

[4] A. Ohtomo, H. Y. Hwang, Nature **2004**, 427, 423.

[5] T. Higuchi, Y. Hotta, T. Susaki, A. Fujimori, H. Y. Hwang, Phys. Rev. B **2009**, 79, 6.

[6] M. Minohara, T. Tachikawa, Y. Nakanishi, Y. Hikita, L. F. Kourkoutis, J.-S. Lee, C.-C. Kao, M. Yoshita, H. Akiyama, C. Bell, H. Y. Hwang, Nano Lett. **2014**, 14, 6743.

[7] J. J. Yang, M. D. Pickett, X. Li, D. A. A. Ohlberg, D. R. Stewart, R. S. Williams, Nat. Nanotechnol. **2008**, 3, 429.

[8] Y. Furubayashi, N. Yamada, Y. Hirose, Y. Yamamoto, M. Otani, T. Hitosugi, T. Shimada, T. Hasegawa, J. Appl. Phys. **2007**, 101, 093705.

[9] B. Oregan M. Gratzel, Nature **1991**, 353, 737.

[10] J. Y. Yang, Y. Sun, P. Lv, L. He, R. F. Dou, C. M. Xiong, J. C. Nie, Appl. Phys. A **2011**, 105, 1017.

[11] K. S. Takahashi, H. Y. Hwang, Appl. Phys. Lett. **2008**, 93, 082112.

[12] S. A. Chambers, C. M. Wang, S. Thevuthasan, T. Droubay, D. E. McCready, A. S. Lea, V. Shutthanandan, C. F. Windisch, Thin Solid Films **2002**, 418, 197.

[13] H. K. Sato, C. Bell, Y. Hikita, H. Y. Hwang, Appl. Phys. Lett. **2013**, 102, 251602.

[14] T. C. Kaspar, S. M. Heald, C. M. Wang, J. D. Bryan, T. Droubay, V. Shutthanandan, S. Thevuthasan, D. E. McCready, A. J. Kellock, D. R. Gamelin, and S. A. Chambers, Phys. Rev. Lett. **2005**, 95, 217203.

[15] T. Tachikawa, M. Minohara, Y. Nakanishi, Y. Hikita, M. Yoshita, H. Akiyama, C. Bell, H. Y. Hwang, Appl. Phys. Lett. **2012**, 101, 022104.

[16] J. Sullivan, S. Erwin, Phys. Rev. B **2003**, 67, 144415.

[17] C. W. Schneider, M. Esposito, I. Marozau, K. Conder, M. Doebeli, Y. Hu, M. Mallepell, A. Wokaun, and T. Lippert, Appl. Phys. Lett. **2010**, 97, 192107.

[18] K. Tanaka, A. Ozaki, J. Catal. **1967**, 8, 1.

[19] X. Q. Gong, A. Selloni, A. Vittadini, J. Phys. Chem. B **2006**, 110, 2804.

[20] G. S. Herman, Y. Gao, T. T. Tran, J. Osterwalder, Surf. Sci. **2000**, 447, 201.

[21] H. Tang, K. Prasad, R. Sanjinès, P. E. Schmid, F. Lévy, J. Appl. Phys. **1994**, 75, 2042.

[22] T. Konaka, M. Sato, H. Asano, and S. Kubo, J. Supercond. **1991**, 4, 283.

[23] Z. Wang, W. Zeng, L. Gu, M. Saito, S. Tsukimoto, Y. Ikuhara, J. Appl. Phys. **2010**, 108, 113701.

[24] D. Souptel, G. Behr, and A. M. Balbashov, J. Cryst. Growth **2002**, 236, 583.

[25] M. L. Reinle-Schmitt, C. Cancellieri, D. Li, D. Fontaine, M. Medarde, E. Pomjakushina, C. W. Schneider, S. Gariglio, P. Ghosez, J. M. Triscone, P. R. Willmott, Nat. Commun. **2012**, 3, 932.

[26] W. Sugimura, A. Yamazaki, H. Shigetani, J. Tanaka, T. Mitsuhashi, Jpn. J. Appl. Phys. **1997**, 36, 7358.

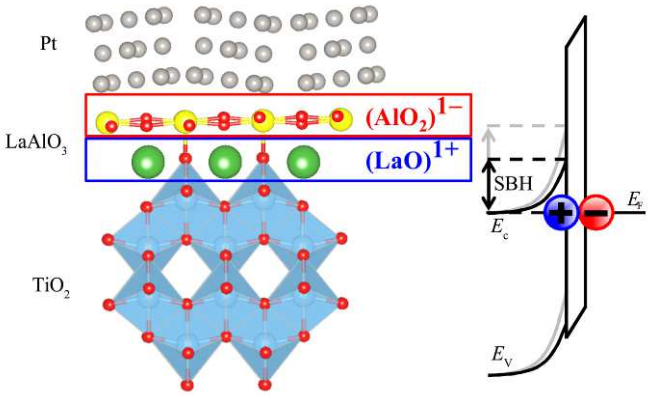

Figure 1. Schematic structure and band diagram of the Pt/$LaAlO_3$/TiO_2 (001) Schottky junctions. E_c and E_v are the conduction band minimum and the valence band maximum of TiO_2 respectively. E_F is the Fermi level of the system. The $LaAlO_3$ (001) substrate under the anatase TiO_2 is not shown.

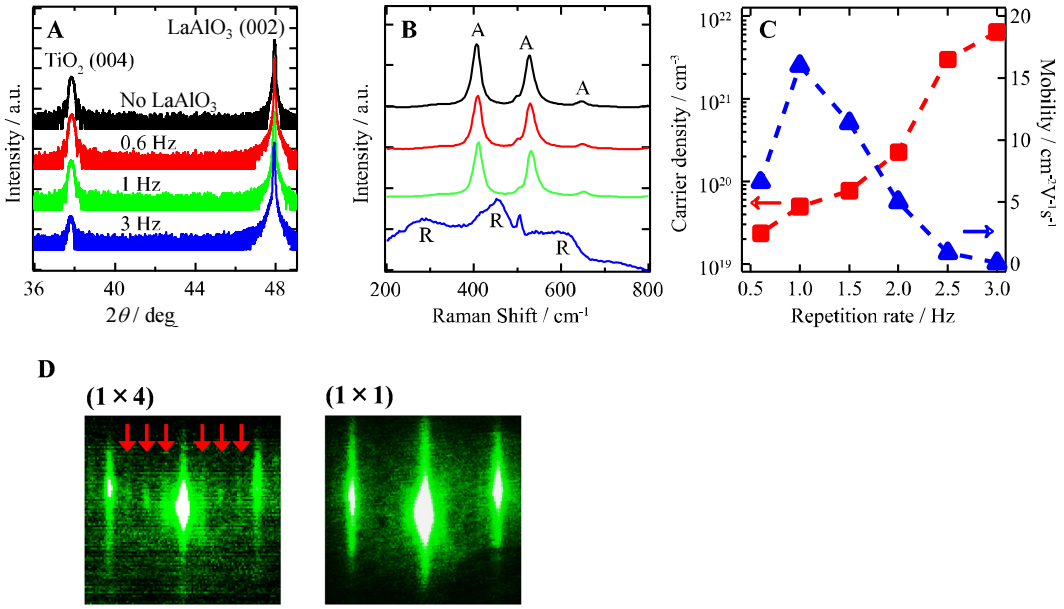

Figure 2. (A) XRD pattern and (B) Raman scattering spectra of $LaAlO_3$ (40 u.c.)/TiO_2 (40 u.c.)/$LaAlO_3$ (001) heterostructures grown at various $LaAlO_3$ laser repetition rates. "A" and "R" in (B) denote Raman scattering peaks characteristic to anatase and rutile respectively. (C) Carrier density and electron mobility of the heterostructure as a function of the repetition rate used for the $LaAlO_3$ layer growth. (D) RHEED patterns of the (1 × 4) reconstruction for as-grown (left) and the (1 × 1) pattern for water-treated (right) TiO_2 films at 600 ºC. The arrows in the (1 × 4) RHEED pattern indicate the additional streaks arising from the reconstruction.

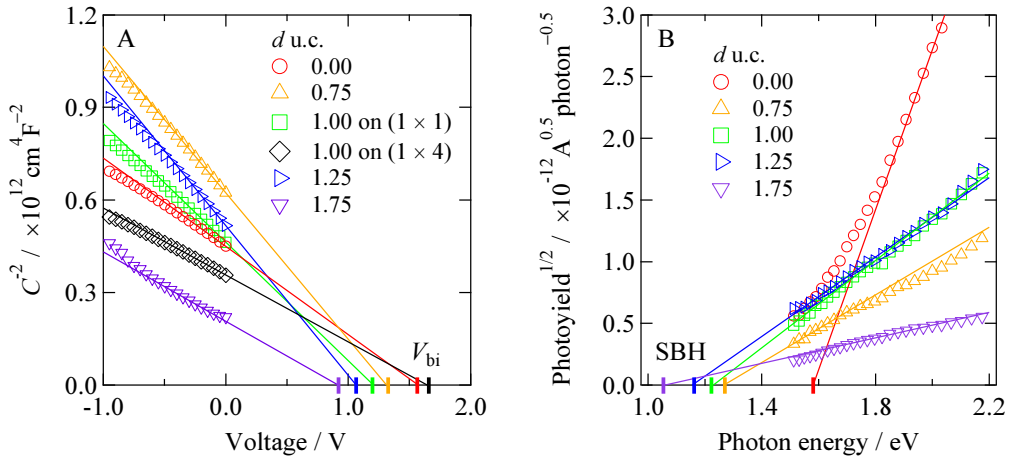

Figure 3. (A) *C-V* data (B) and IPE spectra of Pt (5 nm)/$LaAlO_3$ (*d* u.c.)/Nb:TiO_2 (40 u.c.)/$LaAlO_3$ (001) Schottky junctions at room temperature. Solid lines are linear extrapolations in both *C-V* data and IPE spectra. V_{bi} and SBH values obtained by these measurements are shown by solid lines crossing the horizontal axis.

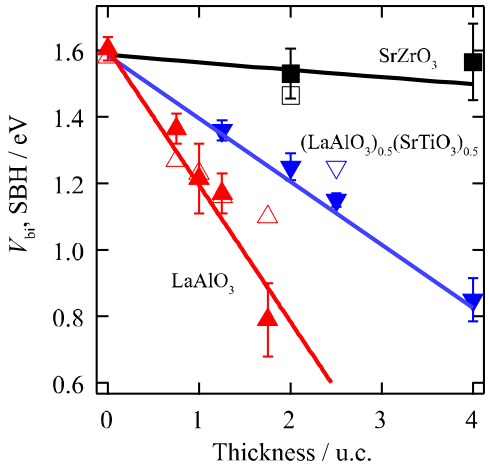

Figure 4. Thickness dependence of V_{bi} (filled symbols) and SBH (open symbols) obtained by *C-V* and IPE measurements for various insertion layers, $LaAlO_3$, $(LaAlO_3)_{0.5}(SrTiO_3)_{0.5}$, and $SrZrO_3$. Solid lines are linear fittings for each data set. The maximum error bars of SBH are within the size of the symbols.

The Schottky barrier heights at the Pt/TiO_2 (001) junctions are modulated over 0.8 eV by insertion of < 1 nm of $LaAlO_3$. The large electric field in the $LaAlO_3$ is stabilized by preserving the continuity of in-plane lattice symmetry at the oxide interface. These results greatly expand the application of dipole engineering to versatile polycrystalline metal/binary oxide functional interfaces.

Keyword transition metal oxides, TiO_2, band alignment, interface dipoles, $LaAlO_3$

Takashi Tachikawa, Makoto Minohara, Yasuyuki Hikita, Christopher Bell, Harold Y. Hwang*

Tuning Band alignment using interface dipoles at the Pt/anatase TiO_2 interface